Journal of Power Sources 248 (2014) 822–830

Contents lists available at ScienceDirect

Journal of Power Sources

journal homepage: www.elsevier.com/locate/jpowsour

Effect of through-plane distribution of polytetrafluoroethylene in carbon paper on in-plane gas permeability

Hiroshi Ito [a,*], Katsuya Abe [b], Masayoshi Ishida [b], Akihiro Nakano [a], Tetsuhiko Maeda [a], Tetsuo Munakata [a], Hironori Nakajima [c], Tatsumi Kitahara [c]

[a] Energy Technology Research Institute, National Institute of Advanced Industrial Science and Technology (AIST), 1-2-1 Namiki, Tsukuba 305-8564, Japan
[b] Department of Engineering Mechanics and Energy, University of Tsukuba, 1-1-1 Tennoudai, Tsukuba 305-8573, Japan
[c] Department of Mechanical Engineering, Kyushu University, 744 Motooka, Nishi-ku, Fukuoka 819-0395, Japan

HIGHLIGHTS

- The through-plane PTFE distribution in GDB was analyzed by SEM–EDS.
- PTFE drying under vacuum condition yielded a relatively uniform PTFE distribution.
- In-plane gas permeability was influenced by the through-plane PTFE distribution.
- The binder distribution in carbon paper was greatly different in Toray and SGL.

ARTICLE INFO

Article history:
Received 13 September 2013
Received in revised form
4 October 2013
Accepted 4 October 2013
Available online 12 October 2013

Keywords:
Proton exchange membrane fuel cell
Gas diffusion backing
Polytetrafluoroethylene
In-plane permeability

ABSTRACT

In-plane permeability of gas diffusion backing (GDB) of proton exchange membrane fuel cells (PEMFCs) was investigated experimentally. Toray-paper and SGL-paper were selected as GDB test samples. Several Toray-papers were treated in-house with polytetrafluoroethylene (PTFE) using the immersion technique, dried either under atmospheric or vacuum pressure, and then sintered. The dependence of PTFE distribution in the through-plane direction on the PTFE drying conditions was examined using scanning electron microscopy (SEM)-based energy dispersive X-ray spectroscopy (EDS) imaging. The EDS image maps revealed that the PTFE distribution strongly depended on the drying condition, and PTFE drying under vacuum pressure yielded a relatively uniform PTFE distribution. The measured in-plane permeability suggests that the homogeneous distribution of PTFE achieved by the vacuum drying produces a porosity-leveling effect. In addition, the relationship between the in-plane permeability and porosity of the Toray-paper samples followed the Kozeny–Carman relation, whereas due to non-fibrous solids such as binder, that of the SGL-paper samples did not.

1. Introduction

During operation of a proton exchange membrane fuel cell (PEMFC), the oxygen reduction reaction rate at the cathode is the limiting kinetic step and determines the maximum operating current density. This rate strongly depends on the transport rate of oxygen from the flow channel to the catalyst sites. Although the electrolyte membrane needs liquid water to retain proton conductivity, the oxygen gas transport can be greatly hindered when liquid water accumulates either in the catalyst layer (CL) or the gas diffusion layer (GDL) of the cathode. Consequently, for optimal water management and performance in PEMFCs, water retention/expulsion properties must be carefully balanced.

The GDL, which is a porous medium located between the CL and the bipolar (flow channel) plate, plays a vital role in this water management. A basal substrate of GDL, called a gas diffusion backing (GDB), is made of either woven carbon cloth or non-woven carbon paper due to their high porosity and electric conductivity [1]. A GDL is generally composed of GDB coated with a hydrophobic microporous layer (MPL), which is usually a mixture of fine carbon particles and a hydrophobic agent. To improve their gas and water transport, GDBs are commonly treated with a hydrophobic agent such as polytetrafluoroethylene (PTFE) to increase the hydrophobicity.

The effect of PTFE content in carbon-paper GDLs without MPL (i.e., GDB) on the PEMFC performance has been experimentally

* Corresponding author.
E-mail address: ito.h@aist.go.jp (H. Ito).

0378-7753/$ – see front matter © 2013 Elsevier B.V. All rights reserved.
http://dx.doi.org/10.1016/j.jpowsour.2013.10.009

examined [1–8]. Studies [2–8] report that adding PTFE to the GDB can enhance the hydrophobicity of pores in the GDB, which can then enhance the cell performance under high humidity conditions, although excessive PTFE loading can reduce the pore size, thus making expulsion of liquid water from the pores more difficult. However, although the loading amount of PTFE was discussed in those studies [2–8], the PTFE distribution throughout the GDB in the through-plane direction was not examined.

Recent several works [1,9–13] have focused on the PTFE through-plane distribution in GDBs. PTFE can be applied to the GDB in several ways. Most commonly, the GDB is dipped into an aqueous PTFE dispersion and excess dispersion is allowed to drip off, then the remaining solvent is removed by oven drying, and finally the PTFE is sintered at above 350 °C. The advantage of this immersion method is that the PTFE loading amount can be controlled by simply adjusting the dispersion concentration. However, uniform distribution of PTFE is difficult to achieve by any PTFE-coating method due to the complex micro pore structure of GDB. Mathias et al. [1] reported that PTFE dispersion drying time can affect its distribution. Based on measurements of PTFE through-plane distribution in relation to PTFE dispersion drying times, they reported that relatively slower drying times yielded higher concentrations in the interior of the GDB, whereas relatively faster drying times yielded higher concentrations near the surface. Inoue et al. [9] supported these observations based on numerical analysis of the evaporation and phase change of PTFE during the drying process. Fishman and Bazylak [10] measured the porosity though-plane distribution of carbon-paper GDB using microscale computed tomography (μCT) imaging. Based on comparison of porosity distribution between GDB samples with and without PTFE treatment, PTFE preferentially accumulated at the local area in through-plane direction near the surface [9]. Rofaiel and Bazylak et al. [11] measured the heterogeneous through-plane PTFE distribution for different types of GDB (paper, felt, and cloth) using scanning electron microscopy (SEM)-based energy dispersive X-ray spectroscopy (EDS) imaging. They reported that the morphological features of untreated GDB significantly affect the PTFE distribution. In addition, Kang et al. [13] focused on the liquid water saturation profile through the GDL (GDB + MPL) obtained by Turhan et al. [14] and Manahan et al. [15] using the neutron radiography (NR) technique. Based on two-phase model calculation results, Kang et al. [13] correlated the profile of liquid water saturation with that of PTFE content throughout the GDB, and reported that the centrally located saturation peaks in the through-plane profile can be attributed to relatively fewer PTFE-coated pores in the inner GDB region.

Mathias et al. [1] suggested that diffusion is typically dominant transport mode in the through-plane direction in a GDL, while convective transport is dominant in the in-plane direction. In particular, mass transfer in an interdigitated flow field is primarily driven by the in-plane permeability, which might also influence significantly the cell performance in a serpentine flow field. Pharoah [16] indicated that the convective transport via the GDB is relevant even when an MPL is added, suggesting that in-plane permeability is a crucial factor in the cell performance in serpentine flow fields. The analytical study of Feser et al. [17] reinforced the importance of the in-plane permeability at the serpentine flow fields. Feser et al. [18] also measured the in-plane permeability of various carbon papers as a function of porosity using either gas or liquid as the working fluid. Gostick et al. [19] examined the permeability of the in-plane and through-plane directions for various types of carbon paper and cloth, and found the in-plane permeability to be twice as high as the through-plane permeability, agreeing with the observation reported by Ihonen et al. [20]. Kitahara et al. [21] also measured the permeability of the in-plane and through-plane directions for carbon-paper GDL with and without MPL, and reported a correlation between the in-plane permeability and the thickness of the MPL penetrating the GDB. Banerjee and Kandlikar [22] reported the in-plane permeability of various GDBs at elevated temperatures up to 90 °C. They [22] also reported that in-plane permeability significantly decreases with PTFE loading. However, no previous studies have considered the correlation between in-plane permeability and the through-plane PTFE distribution.

Our goal in the present study was to verify the relationship between the in-plane permeability of a carbon-paper GDB and the through-plane distribution of PTFE. We did this by examining the effect of different drying conditions of PTFE dispersion on PTFE distribution in carbon-paper GDB by using EDS analysis. First, carbon-paper GDB samples were prepared using the immersion technique in which PTFE was loaded under different drying conditions, namely, vacuum pressure (vacuum-dried) and atmospheric pressure (air-dried), because previous studies pointed out [1,9] that this drying process is important for controlling the PTFE distribution in the through-plane direction of the GDB substrates. Then, the in-plane permeability of the samples was determined and compared with samples without PTFE loading. Finally, the relationship between in-plane permeability and porosity of the samples was evaluated based on the Kozeny–Carman relation.

2. Experiments

2.1. Sample preparation

Three commercial products available for carbon-paper GDBs of PEMFCs were selected for comparison and did not have any additional layer such as an MPL: Toray-paper (TGP-H-090) and SGL-paper (34AA and 34BA). A total of five samples were prepared as summarized in Table 1: (1) Toray-paper not treated with PTFE (sample CT0), (2) Toray-paper treated with PTFE under air drying conditions (CT1), (3) Toray-paper treated with PTFE under vacuum drying conditions (CT2), (4) SGL34AA not treated with PTFE (CS0), and (5) SGL34BA loaded 5 wt.% PTFE (CS1). Note that the PTFE treatment process for SGL34BA is unknown because PTFE was applied by the manufacturer. PTFE treatment for the Toray-paper samples (50 × 50 mm) was executed in-house as follows. Each sample was dipped into a 10 wt.% PTFE dispersion (D-210C, Daikin) for about 2 min, and then placed on a needle-point holder (Fig. 1). The size of PTFE particles in the dispersion is about 0.20 μm, which is sufficiently small compared with the fiber diameter (7–9 μm) or the pore diameter (>1 μm) of Toray-paper. The holder with the sample was immediately placed in a drying oven (VT220, Etak) at room temperature, and the oven was then heated immediately after the door was closed. (Due to its needle points, this holder allowed excess dispersion to drip off easily from the GDB during this drying process.) The oven was then heated to 100 °C in about

Table 1
GDB materials and properties in the present study.

Notation	Material	Initial porosity (ε_0)	Initial thickness (h_0) [μm]	PTFE loading [wt.%]	PTFE drying condition
CT0	Toray 090	0.762	305	–	–
CT1	Toray 090	0.724	305	14.6	Air
CT2	Toray 090	0.719	305	14.3	Vacuum
CS0	SGL34AA	0.812	283	–	–
CS1	SGL34BA	0.809	292	5	

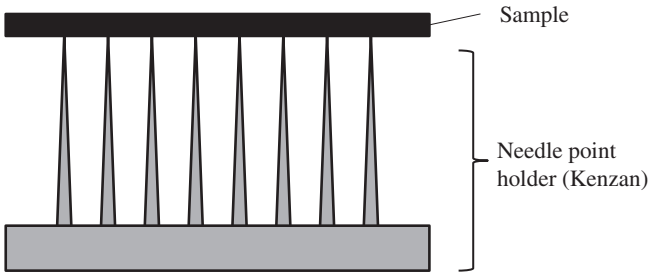

Fig. 1. Schematic view of PTFE drying set-up for GDB samples.

30 min, then kept at that temperature for 1 h, after which the heating was turned off. The sample was left in the oven for over 10 h until the oven reached room temperature. For the air-drying condition, the oven was open to the air through a pipe, although the door was closed. For the vacuum-drying, the air in the oven was evacuated just after the door was closed, and the pressure was kept at vacuum less than 0.1 kPa until the door was opened after the oven reached room temperature. After either drying process, the samples were transferred to another oven and sintered at 360 °C for 1 h under vacuum conditions (less than 0.03 kPa).

For EDS analysis, a fragment of each sample was obtained from the same base substrate of GDB as the permeability measurement (described in Section 2.4). Each fragment sample was first frozen using liquid nitrogen and then immediately cut with a knife to reveal a sharp cross-section.

2.2. Initial thickness and porosity of GDB

Initial thickness of each sample (h_0) was measured with a thickness gauge that can measure thickness under quite low compression (less than 1.5 N) with an accuracy of ±3 μm. The measured h_0 of SGL-papers (34AA and 34BA) agreed with the manufacturer's specifications, whereas that of Toray-paper (090) was significantly higher (305 μm vs 280 μm, respectively).

Initial bulk porosity of the samples (ε_0) was also measured by weighing the sample before and after immersion in a wetting liquid, decane, which has low surface tension (23.4 mN m^{-1}) and thus has the ability to fill all pores. To ensure complete intrusion of the liquid into the pores, the immersed sample was placed in a vacuum chamber for about 10 min before the final weighing. Table 1 summarizes these measured properties of the GDB samples.

2.3. Energy dispersive X-ray spectroscopy (EDS) analysis

SEM imaging (JEOL JSM-7400F SEM) and EDS maps of the cross-sectional images of each carbon-paper GDB were used to quantify the fluorine (F) content of the GDB, because, as Rofaiel et al. [11] reported, F is a suitable element for determining the presence of PTFE throughout the GDB due to its high concentration in PTFE and its absence in carbon-paper GDB. The SEM magnification was 100×, and the spatial resolution for the EDS map was about 5 μm. The total size of the EDS image was 256 pixels in in-plane direction, whereas in through-plane direction, it varied between 50 and 70 pixels depending on the sample thickness. The F map images were treated and analyzed using an image translation program (Image J) as follows. First, the noise was removed from the raw grayscale image, based on a commonly set threshold noise value of 2 in the overall grayscale value of 255. Then, the grayscale value of each pixel along the in-plane direction of the image (horizontal axis in the EDS map) was summed to obtain a relative PTFE value along the thickness of the GDB. Finally, the relative F (i.e., relative PTFE) values were normalized across the through-plane direction (z).

2.4. Measurement of pressure drop and flow rate to determine in-plane gas permeability

The in-plane permeability k_i of each GDB sample was obtained by measuring the pressure drop and flow rate through the samples using a radial flow apparatus (Fig. 2(a)) similar to that used by Feser et al. [18] and Kitahara et al. [21]. An annular GDB sample (14 mm o.d. × 8 mm i.d.) (Fig. 2(b)) was placed and then compressed between two cylindrical plates whose spacing was controlled by an annular stainless steel or carbon steel spacer of known thickness (h). A soft O-ring was used for gas sealing between the plates. (Note that the force required to deform the O-ring was negligible compared with the compression force acting on the GDB sample even when a spacer was in place.) A torque wrench was used to tighten the four bolts of the plates to a torque of 5 Nm each. This torque was confirmed sufficiently high so that both the sample and spacer were rigid and the results did not depend on the torque.

The k_i measurement was performed at room temperature as follows. The working fluid was air supplied from a compressor and dried with a membrane dryer before entering the test section at flow rate Q, which was measured on the inlet side using a digital flow meter (SEF-F40, Horiba). The dew point of the working air was less than −20 °C at atmospheric pressure. A differential pressure transducer (either DP45 and DP15, Validyne, depending on the differential pressure range in the measurement) was connected to the inlet to measure the pressure difference between the inlet and outlet ($\Delta P = P_i - P_o$). One side of the pressure transducer was connected to the inlet line and the other side was open to the air. Preliminary experiments confirmed that the pressure difference (ΔP) of the test section in the absence of a sample was negligible over the entire range of Q (0–200 mL min^{-1}) studied here. The barometric pressure was monitored by a manometer and used in the analysis to determine k_i.

Measurements were repeated three times for Toray-papers (CT0, CT1, and CT2) and twice for SGL-papers (CS0 and CS1).

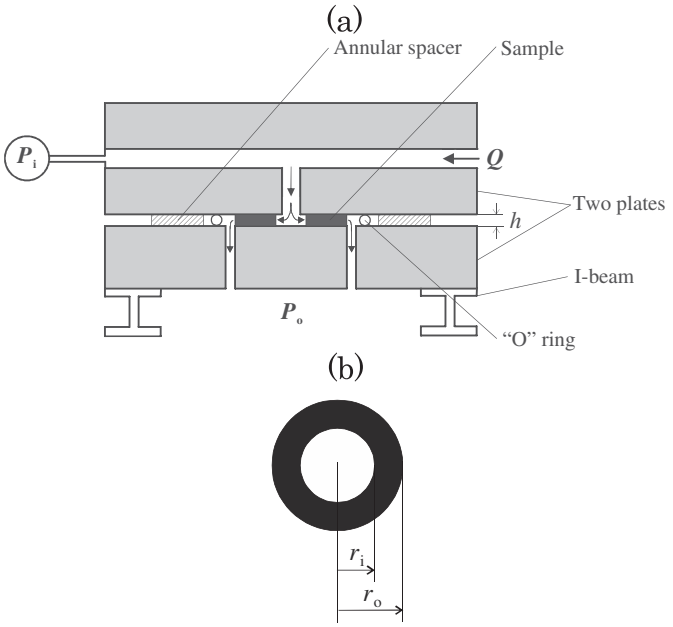

Fig. 2. (a) Schematic of radial flow apparatus to determine in-plane permeability and (b) geometry of a sample with r_o = 7 mm and r_i = 4 mm.

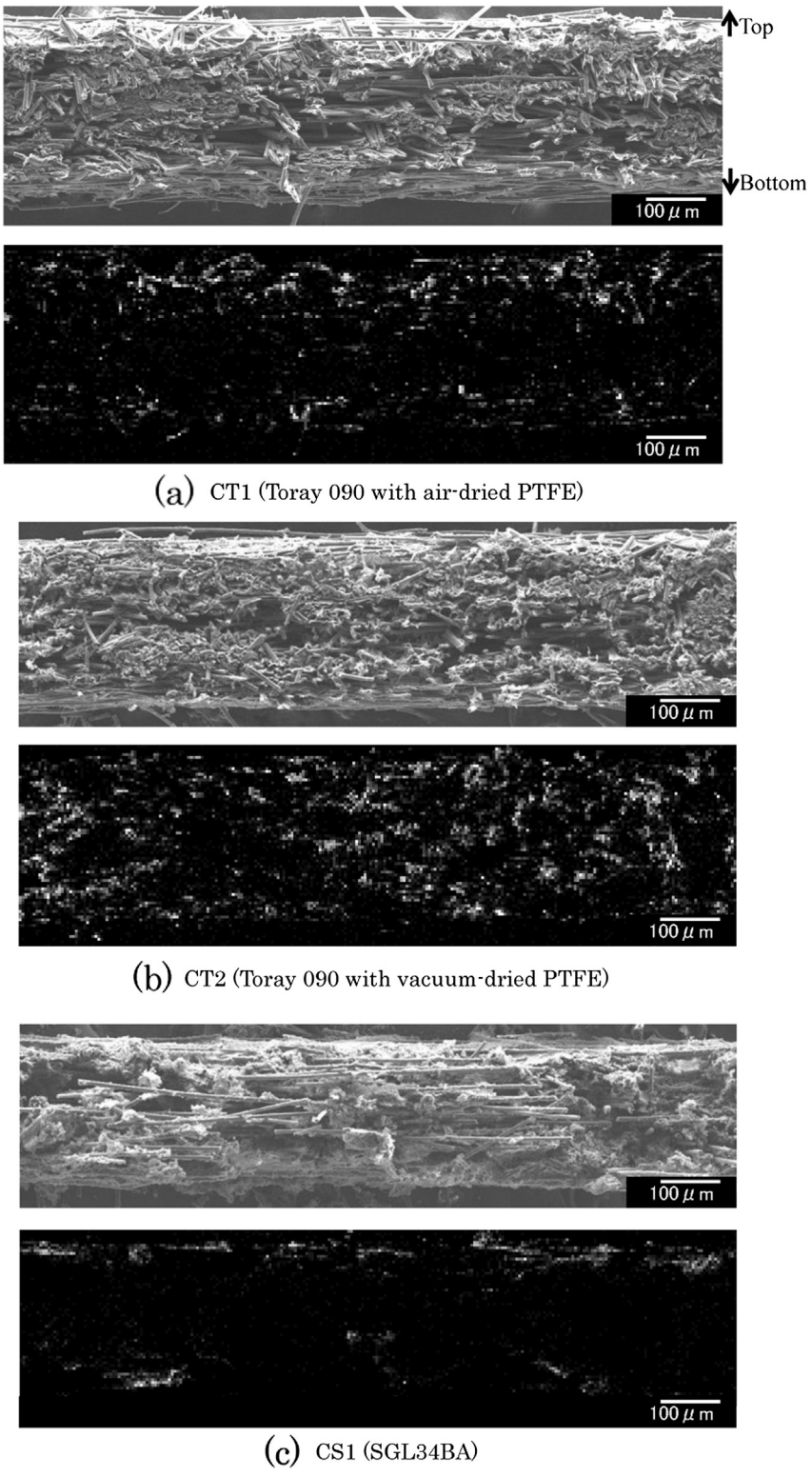

Fig. 3. SEM image (upper) and corresponding EDS map of fluorine (F) (bottom) of cross-section of samples (a) CT1 (Toray 090 with air-dried PTFE), (b) CT2 (Toray 090 with vacuum-dried PTFE), and (c) CS1 (SGL34BA).

The Q was kept constant for at least 2 min for each measurement. Signals from the pressure transducer (i.e., ΔP) and the flow meter (i.e., Q) were amplified and acquired every 0.5 s for 30 s at a stable state, and the average values of ΔP and Q were used to determine k_i.

2.5. Data analysis to determine in-plane gas permeability k_i

The measured ΔP and Q were used to determine k_i with the model developed by Feser et al. [18] for radial flow permeability and incorporates fluid compressibility. The model assumes k_i is

homogeneous and transversely isotropic. In the case of nonwoven filter media such as carbon paper, the pore structure is sufficiently small that concerns of a high Reynolds number and related turbulence generally are not valid, and therefore Darcy's law can be applied. For example, if we assume the pore size (d) is 10 μm, then the maximum Reynolds number ($=\rho v d/\mu$) would be about 0.6 for the flow velocity (v) in the present measurement conditions.

In this study, we used our measured ΔP and measured Q in the following relation derived by Feser et al. [18] to calculate k_i:

$$Q = \frac{\pi k_i h}{\mu \ln(r_o/r_i)} \frac{P_i^2 - P_o^2}{P_o} \quad (1)$$

where h is the thickness of the GDB sample (i.e., spacer thickness), μ is the viscosity of the working fluid (air), P_i the absolute pressure at the inlet, and P_o is the absolute pressure at the outlet (P_o = atmospheric pressure in our study), and r_i, and r_o are the inner radius and outer radius of the sample, respectively (see Fig. 2).

3. Results and discussion

3.1. EDS analysis results

Fig. 3 shows cross-sectional SEM images and corresponding EDS maps for F of (a) CT1 (air-dried PTFE), (b) CT2 (vacuum-dried PTFE), and (c) CS1 (SGL34BA) samples. The upper side of the images in Fig. 3(a) and (b) corresponds to the top of the sample during the PTFE drying treatment; atmospheric drying for CT1 and vacuum for CT2 (see Section 2.1 and Fig. 1). Comparison of the EDS maps for F for these CT1 and CT2 (Fig. 3(a) and (b)) reveal a significant difference in the PTFE distribution. For CT1, PTFE was heterogeneously localized near both the upper and lower surfaces, whereas for CT2, PTFE was distributed more homogeneously throughout the bulk. Note that the total amount of PTFE loading was similar for both of these samples (Table 1). For CS1 (Fig. 3(c)), the PTFE distribution was similar to that for CT1, namely, heterogeneously localized near both surfaces.

Fig. 4 shows the through-plane distributions of the PTFE fraction (f_{PTFE}) calculated from the EDS maps for samples CT1, CT2, and CS1. Here, f_{PTFE} distributions were averaged along the in-plane direction of the EDS images (horizontal axes in Fig. 3). Because the summed total of f_{PTFE} was normalized to 1 for these three samples, these distribution plots do not provide a quantitative analysis of the actual PTFE content in the through-plane direction. Fig. 4(a) shows the resulting bimodal PTFE distribution for CT1 (air-dried PTFE in Fig. 3(a)). Based on the through-plane ε distribution of Toray-papers that they measured using the μCT technique, Fishman and Bazylak [10] attributed the existence of local ε minima near the surface in the Toray-paper to the high concentration of binder material. (However, the reason of heterogeneous binder distribution in untreated Toray-papers is not clear, because there is a lot of stages in the carbon paper making process [1], such as paper-making, resin impregnation, molding, and carbonization.) In addition, when they applied PTFE to the Toray-paper, PTFE preferentially agglomerated at the same through-plane location as the binder material [10]. They concluded that the PTFE through-plane distribution was similar to the ε distribution in the Toray-paper. Because all Toray-paper samples (including PTFE-treated) that they tested were purchased from commercial venders, the process of PTFE treatment was unknown.

The PTFE distribution in CT2 (vacuum-dried PTFE) significantly differed (Fig. 4(b)) from that in CT1 (Fig. 4(a)). Due to the vacuum drying, capillary pressure had no effect on the agglomeration mechanism of PTFE, and thus the PTFE in CT2 was distributed more evenly throughout the bulk. Mathias et al. [1] reported that PTFE

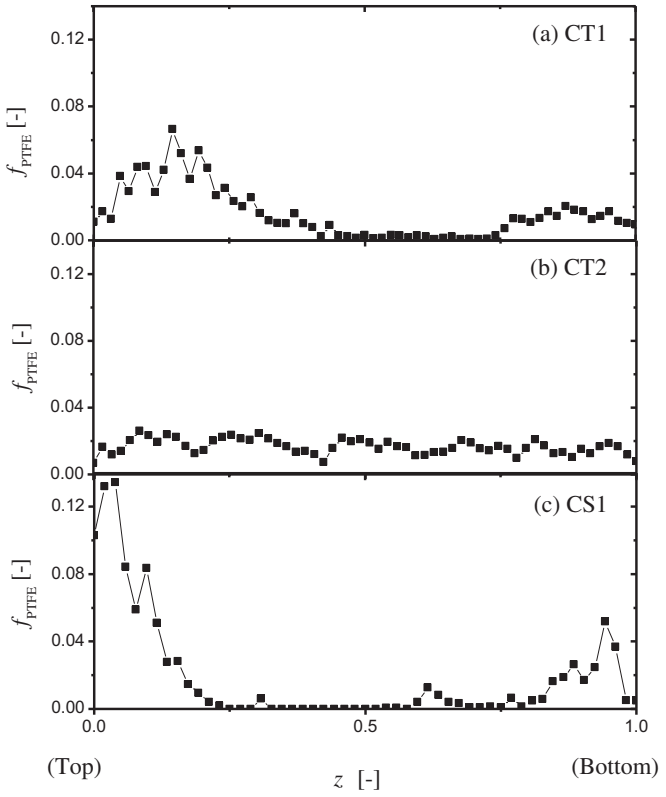

Fig. 4. Through-plane PTFE distribution calculated from EDS map of F (Fig. 3) along relative thickness of GDB (z) from top (0) to bottom (1) for samples (a) CT1, (b) CT2, and (c) CS1.

dispersion drying time can affect its distribution. In our current study, the temperature hysteresis during all PTFE treatments was the same in both air and vacuum drying conditions. Therefore, PTFE-dispersion drying rate was not a factor in the through-plane PTFE distribution. The difference in through-plane PTFE distribution between CT1 and CT2 can be thus attributed only to the pressure conditions during drying, namely, atmospheric or vacuum.

The bimodal PTFE distribution for CS1 (Fig. 4(c)) is similar to that for CT1 (Fig. 4(a)). PTFE was highly concentrated near both the upper and lower surfaces of the GDB (as indicated by the two sharp peaks), but only slightly in the interior. This bimodal distribution of PTFE suggests that the drying process of PTFE was carried out under atmospheric conditions the same as for CT1.

The model simulation results of Kang et al. [13] indicates that the bimodal distribution of PTFE would tend to produce the centrally located liquid saturation peaks in the through-plane direction and cause higher saturation level compared with the uniform distribution as a whole of GDL. Thus, it can be suggested that the uniform PTFE distribution in the through-plane direction is more favorable to efficient discharge of liquid water through the GDL rather than the bimodal distribution.

3.2. In-plane permeability k_i

The relationships of ΔP and Q were measured with the above mentioned apparatus (Section 2.4) changing the spacer thickness. Fig. 5 shows typical data obtained with CT0 (untreated Toray 090). For this sample, ΔP and Q showed a linear relationship over the entire range of Q. To validate these measurements and data analysis, the relationship between calculated k_i and ε of CT0 was

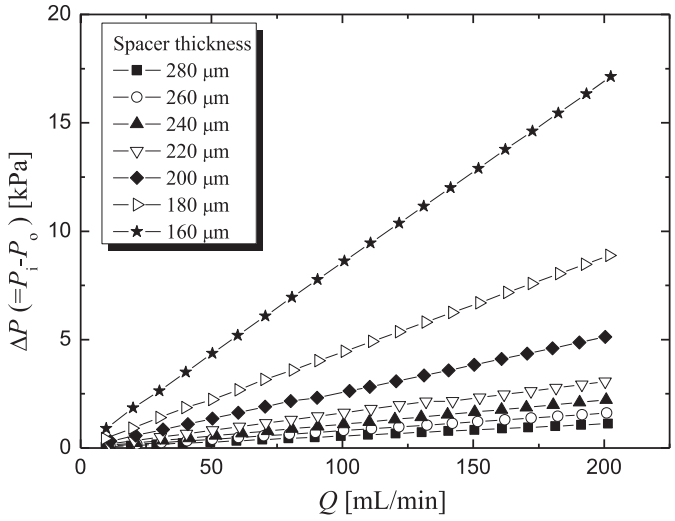

Fig. 5. Measured in-plane pressure difference (ΔP) as a function of flow rate of air (Q) for CT0 (untreated Toray 090) compressed to different thickness.

compared with reference data from the literature using the following equation to determine ε:

$$\varepsilon = 1 - \frac{h_0}{h}(1 - \varepsilon_0) \tag{2}$$

where h_0 is the initial thickness of the sample, ε_0 is the initial porosity. Fig. 6 shows the comparison, revealing that, at a given ε, k_i from our current study is higher than that from reference data. The thickness range of the spacers (h) used in our study (160–280 μm) was similar to that used by Gostick et al. [19] (150–270 μm), and the resulting k_i range was also similar. Therefore, the difference in permeability at a given ε between these studies is mainly due to the difference in h_0 and ε_0. The effects of ε_0 are quite significant. Table 2 summarizes a survey of ε data in the literature [5–7,10,18,19,23,24]. The manufacturer's specifications for ε_0 is typically 0.78 for Toray 060, 090 and 120, indicating that the manufacturing process and resulting structure of these three papers are the same. The reference data for k_i in Fig. 6 [18,19] were based on a relatively high ε_0 (0.80), although the literature data vary widely between 0.72 and

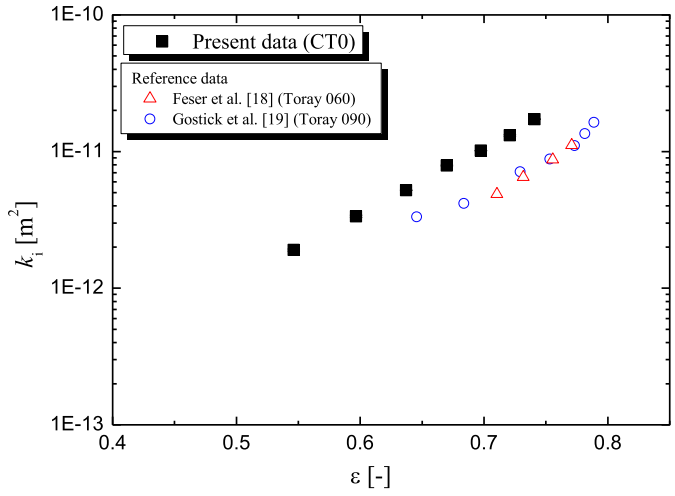

Fig. 6. Measured in-plane permeability (k_i) vs porosity (ε) for CT0 (untreated Toray 090) compared with literature data. (Present data include error bars.)

Table 2
Literature data of initial bulk porosity ε_0 measured for untreated Toray papers.

Reference	Sample	Porosity (ε_0)	Technique
Williams et al. (2004) [23]	Toray 120	0.756	MIP[a]
		0.759	Decane weighing
Park et al. (2004) [5]	Toray 060	0.777	
	Toray 090	0.721	
Benziger et al. (2005) [6]	Toray 120	0.72	Kerosene weighing
Feser et al. (2006) [18]	Toray 060	0.80[b]	
Gostick et al. (2006) [19]	Toray 090	0.80	MIP[a]
Lobato et al. (2008) [7]	Toray 120	0.763	MIP[a]
Zamel et al. (2010) [24]	Toray 120	0.755	
Fishman et al. (2011) [10]	Toray 090	0.826	X-ray μCT visualization
	Toray 120	0.793[c]	

[a] Mercury intrusion porosimetry.
[b] Estimated value from presented data of compression rate and porosity.
[c] Average value of repeated twice measurements.

0.83. Consequently, due to such variation, it cannot be determined whether the distribution in the ε data is due to measurement error or to lot-to-lot variation within the commercial manufacturing process. Among the literature, the study of Williams et al. [23] is noteworthy, because they determined ε of several carbon papers by applying two different methods: the MIP method, and the immersion method that we used in the present study. They [23] reported good agreement between the two methods for all samples, including Toray and SGL papers, with a difference of less than 3.5%. Our measured ε_0 must therefore be reliable, because it is relatively close to that reported by Williams et al. [23]. In addition, if the ε_0 value of 0.80 presented by Gostick et al. [19] was applied to Eq. (2), our data in Fig. 6 would be shifted to the right (i.e., higher ε), and thus approach the reference data. In conclusion, our measurements of ΔP and Q and their data analysis were appropriate for evaluating the k_i of GDB.

Fig. 7(a) and (b) shows k_i–ε characteristics for the Toray and SGL papers, respectively. In the case of Toray papers (Fig. 7(a)), k_i of CT1 was higher than that of CT0, even though PTFE was loaded. The ε_0 of CT1 was lower than that of CT0 due to PTFE loading (Table 1). The lower ε caused by PTFE loading did not effectively hinder gas permeation compared to hindrance by compression of the paper. Therefore, k_i of CT1 was apparently higher at a given ε. In contrast, k_i of CT2 was significantly lower than that of CT1, even though both CT1 and CT2 had similar PTFE-loading in total bulk and had similar ε_0. The difference in k_i of CT1 and CT2 can therefore be attributed to the difference in PTFE distribution in the through-plane direction as shown in Figs. 3 and 4. Toray-paper is known to have a heterogeneous ε distribution in the through-plane direction and have local minima of ε near both the upper and lower surfaces due to high concentration of binder material [25]. Fishman and Bazylak [10] investigated the change in the ε distribution caused by PTFE loading with Toray-paper. They found that the decrease in ε was mainly observed at the local minima near both surfaces (surface region), and that ε in the central (core) region remained relatively high. Although the PTFE-treatment process of the sample used by Fishman and Bazylak [10] was not clear, it must be similar to that of CT1 in our study, because the loaded PTFE was observed locally near both surfaces. Based on the k_i obtained here and the ε distribution observed by Fishman and Bazylak [10], it is suggested that, not only in CT1 but also in CT0, the gas flow in the in-plane direction mainly passes through the central region of GDB. Therefore, the local decrease in ε at the surface region was not highly effective for in-plane permeation. However, in CT2, because the PTFE was homogenously distributed in the through-plane direction, gas permeation would be hindered throughout the entire region and

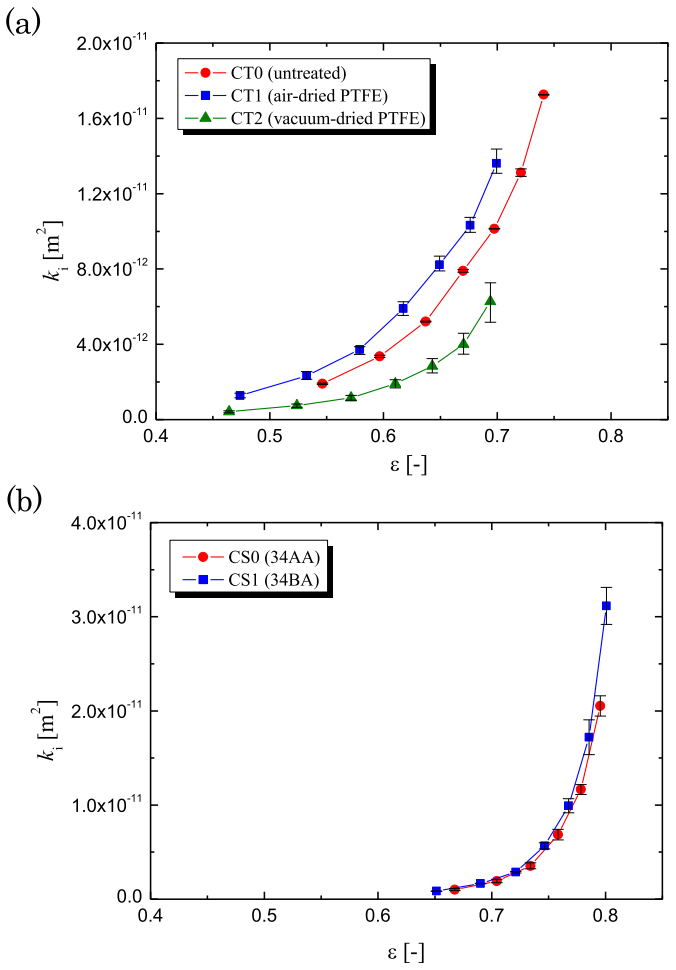

Fig. 7. In-plane permeability (k_i, linear scale) vs porosity (ε) of samples of (a) Toray papers and (b) SGL papers.

thus k_i was decreased significantly. Consequently, the homogeneous distribution of PTFE achieved by the vacuum drying produces a porosity leveling, which means porosity profile of PTFE treated sample became more flat in the through-plane direction compared to that of untreated sample. In the case of SGL paper (Fig. 7(b)), the measured k_i for untreated (CS0) and treated (CS1) GDBs agree with each other, which can be explained as follows.

The relationship between k_i and ε is often described by the Kozeny–Carman equation [19,26,27]:

$$k_i = K_C \frac{\varepsilon^3}{(1-\varepsilon)^2} \tag{3}$$

where K_C is the Kozeny–Carman constant. The Kozeny–Carman model was originally developed for fluid flowing through a packed bed of solids. Although a more detailed equation of the Kozeny–Carman model including the fiber diameter [19,27] or tortuosity factor [26] of the media has been applied previously, here we adopted the simplified equation of Eq. (3) to grasp the overall relation between measured data and the model. Fig. 8(a) and (b) shows the measured k_i–ε characteristics were compared to the Kozeny–Carman relation, and Table 3 lists the fitted values of K_C. The k_i–ε of CT0 and CT1 is fitted relatively well by the Kozeny–Carman, whereas that of CT2 deviates from the model at low ε region (coefficient of correlation, R^2, was relatively small as shown in Table 3). As for SGL papers (CS0 and CS1), the k_i–ε cannot be fitted appropriately by the Kozeny–Carman relation. Feser et al. [18] also reported that the k_i–ε plots of untreated Toray paper (060) follow the Kozeny–Carman equation quite closely, whereas that of SGL paper (31BA) does not. Fig. 9 shows magnified SEM images of the center region in the cross-section of the three samples (CT1, CT2, CS0), revealing distinct differences in their solid structure composed of carbon fibers, binder, and PTFE. In the case of CT1 (Fig. 9(a)), the central area contained mostly carbon fibers, because the PTFE was heterogeneously distributed near both surfaces as shown in Figs. 3(a) and 4(a). In addition, the binder material was apparently also heterogeneously distributed near both surfaces, as reported by Fishman and Bazylak [10]. In the case of CT2 (Fig. 9(b)), non-fibrous solids appear along with fibers, and were identified as PTFE by X-ray diffraction. In this sample, the PTFE was homogeneously distributed throughout the entire sample in the through-plane direction as shown in Figs. 3(b) and 4(b). In the case of CS0 (Fig. 9(c)), the fibers were covered significantly by non-fibrous material identified as binder. In this sample, considerable amount of non-fibrous binder was distributed homogeneously throughout the entire sample in the through-plane direction. (Note: Because the binder distribution was the same in both CS1 and CS0, Fig. 3(c) is an image of CS1.) Based on comparison of the k_i–ε relationship (Fig. 8) and observation of the fiber structure of the samples of CT2 and CS0 (Fig. 9), deviation from the Kozeny–Carman equation can be attributed to the existence of non-fibrous solid (PTFE or binder).

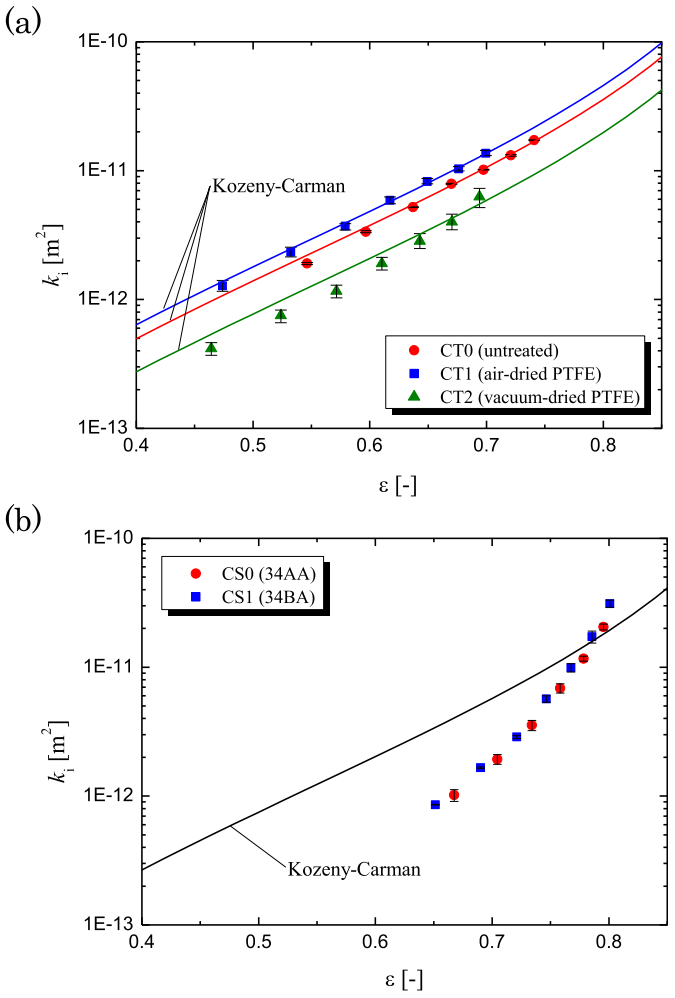

Fig. 8. In-plane permeability (k_i, logarithm scale) vs porosity (ε) of samples of (a) Toray papers and (b) SGL papers. Solid lines represent fitted lines using the Kozeny–Carman model expressed as Eq. (3).

Table 3
Kozeny–Carman constant K_C and coefficient of correlation R^2 obtained by fitting calculation as shown in Fig. 9.

Material notation	Kozeny–Carman constant (K_C) [m^2]	Coefficient of correlation (R^2)
CT0	2.785×10^{-12}	0.997
CT1	3.579×10^{-12}	0.998
CT2	1.543×10^{-12}	0.954
CS0/CS1	1.500×10^{-12}	0.722

The Kozeny–Carman equation must therefore be valid only for fibrous structure. In the cases of CT0 and CT1, because non-fibrous solids (not only PTFE but also binder) were localized near both surfaces in the through-plane direction and the fibrous structure was maintained in the central region, the gas (air) permeation through the fibrous structure was kept within the central region even when the sample was compressed, and thus the k_i–ε relationship for these two samples followed the Kozeny–Carman equation. However, in the cases of CT2, as the sample was compressed (i.e., ε decreased), the effect of uniformly distributed non-fibrous PTFE became significant, and the k_i–ε relationship deviated from the Kozeny–Carman equation. This effect of non-fibrous PTFE distribution explains the low k_i for CT2, and thus reinforces the hypothesis of porosity leveling by the homogeneous PTFE distribution discussed above. In the cases of SGL papers (CS0 and CS1), deviation from the Kozeny–Carman relation equation can be attributed not to the PTFE but to the binder, because these samples contained a considerable amount of binder, and thus comparison between CS0 and CS1 reveals a negligible effect of PTFE loading on the k_i–ε relationship for SGL paper. We tried to apply two other empirical correlations describing the relation between k_i and ε in fiber structures proposed by Davies [26,28] and Tomadakis and Sotirchos [19,29] for the data of SGL papers. However, neither of the correlations could fit appropriately the relation of CS0 and CS1.

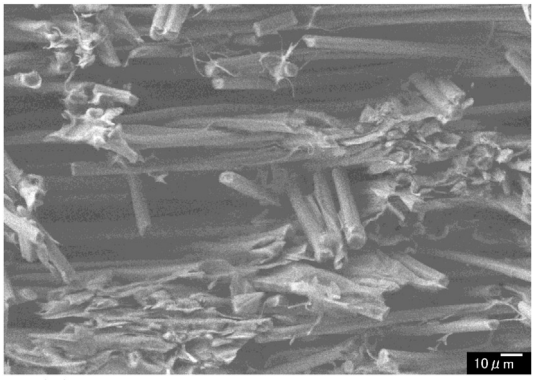

(a) CT1 (Toray 090 with air-dried PTFE)

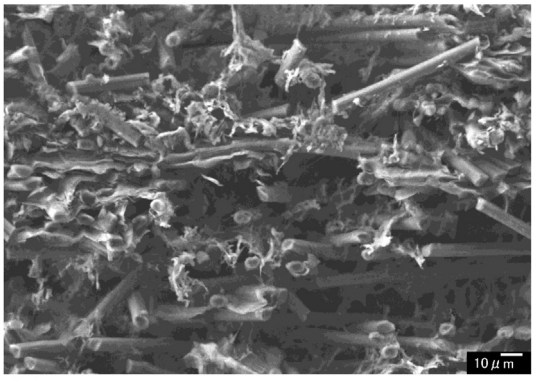

(b) CT2 (Toray 090 with vacuum-dried PTFE)

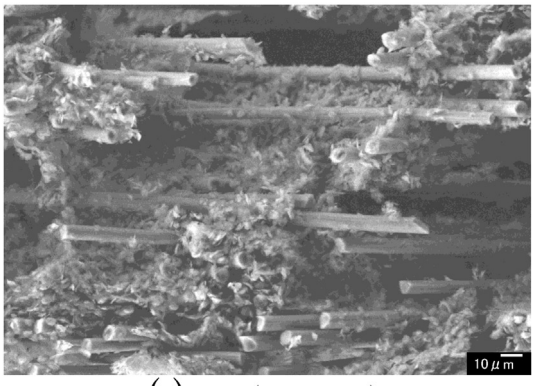

(c) CS0 (SGL34AA)

Fig. 9. Magnified SEM image of central region of GDB cross-section of samples (a) CT1 (Toray 090 with air-dried PTFE), (b) CT2 (Toray 090 with vacuum-dried PTFE), and (c) CS0 (SGL34AA).

4. Conclusions

In this study, we investigated the in-plane permeability of GDBs of PEMFCs using Toray-paper (TGP-H-090) and SGL-paper (34AA and 34BA) as the GDBs. Some of the Toray-papers were treated with PTFE using the immersion technique where the sample was immersed in PTFE dispersion, then dried either at atmospheric or vacuum pressure, and then sintered. The dependence of PTFE distribution on the PTFE drying conditions was examined using SEM–EDS analysis. The EDS image maps revealed that the PTFE distribution strongly depended on the drying condition; PTFE-drying under atmospheric pressure created highly heterogeneous PTFE distributions in the through-plane direction, with high concentrations near both the upper and lower surfaces, whereas PTFE-drying under vacuum pressure created a relatively uniform PTFE distribution.

The in-plane permeability (k_i) of GDB was obtained by radial permeability experiments. At a given total amount of loaded PTFE, the k_i of PTFE-treated GDB with vacuum drying was significantly lower than that with air drying. This difference suggests that the homogeneous distribution of PTFE achieved by the vacuum drying produces a porosity-leveling effect. In addition, the relationship between the k_i and porosity (ε) was investigated using the Kozeny–Carman relation. The k_i–ε relationship of Toray-papers followed the Kozeny–Carman relation, whereas that of SGL-papers did not. This difference suggests that non-fibrous solids (PTFE or binder) play a crucial role in the k_i–ε relationship.

Acknowledgment

The authors gratefully acknowledge the financial support from the Ministry of Economy, Trade and Industry (METI) of Japan under the Japan-U.S. Cooperation Project for Research and Standardization of Clean Energy Technologies and Japan Science and Technology Agency (JST) under the Strategic Japanese–Chinese Joint Research Program for Highly-efficient Energy Utilization. The authors also thank Dr. Satoshi Someya (AIST) for helpful discussion on imaging and thank Mr. Akira Takatuski (AIST) for his SEM–EDS expertise.

References

[1] M.F. Mathias, J. Roth, J. Fleming, W. Lehnert, in: W. Vielstich, A. Lamm, H.A. Gasteiger (Eds.), Handbook of Fuel Cells, vol. 3, John Wiley and Sons, West Sussex, 2003 (Chapter 46).

[2] J. Moreira, A.L. Ocampo, P.J. Sebastian, M.A. Smit, M.D. Salazar, P. del Angel, J.A. Montoya, R. Pérez, L. Martínez, Int. J. Hydrogen Energy 28 (2003) 625–627.
[3] G. Lin, V. Nguyen, J. Electrochem. Soc. 152 (2005) A1942–A1948.
[4] C. Lim, C.Y. Wang, Electrochim. Acta 49 (2004) 4149–4156.
[5] G.G. Park, Y.J. Sohn, T.H. Yang, Y.G. Yoon, W.Y. Lee, C.S. Kim, J. Power Sources 131 (2004) 182–187.
[6] J. Benziger, J. Nehlsen, D. Blackwell, T. Brennan, J. Itescu, J. Membr. Sci. 261 (2005) 98–106.
[7] J. Lobato, P. Cañizares, M.A. Rodrigo, C. Ruiz-Lopez, J.J. Linares, J. Appl. Electrochem. 38 (2008) 793–802.
[8] Y.I. Chou, Z.Y. Siao, Y.F. Chen, L.Y. Sung, W.M. Yang, C.C. Wang, J. Power Sources 195 (2010) 536–540.
[9] G. Inoue, N. Ishibe, Y. Matsunuma, M. Minemoto, ECS Trans. 50 (2) (2012) 461–468.
[10] Z. Fishman, A. Bazylak, J. Electrochem. Soc. 158 (2011) B841–B845.
[11] A. Rofaiel, J.S. Ellis, P.R. Challa, A. Bazylak, J. Power Sources 201 (2012) 219–225.
[12] R.J.F. Kumar, V. Radhakrishnan, P. Haridoss, Int. J. Hydrogen Energy 37 (2012) 10830–10835.
[13] K. Kang, K. Oh, S. Park, A. Jo, H. Ju, J. Power Sources 212 (2012) 93–99.
[14] A. Turhan, S. Kim, M. Hatzell, M.M. Mench, Electrochim. Acta 55 (2010) 2734–2745.
[15] M.P. Manahan, M.C. Hatzell, E.C. Kumbur, M.M. Mench, J. Power Sources 196 (2011) 5573–5582.
[16] J.G. Pharoah, J. Power Sources 144 (2005) 77–82.
[17] J.P. Feser, A.K. Prasad, S.G. Advani, J. Power Sources 161 (2006) 404–412.
[18] J.P. Feser, A.K. Prasad, S.G. Advani, J. Power Sources 162 (2006) 1226–1231.
[19] J.T. Gostick, M.W. Fowler, M.D. Pritzker, M.A. Ioannidis, L.M. Behra, J. Power Sources 162 (2006) 228–238.
[20] J. Ihonen, M. Mikkola, G. Lindberg, J. Electrochem. Soc. 151 (2004) A1152–A1161.
[21] T. Kitahara, T. Konomi, H. Nakajima, J. Power Sources 195 (2010) 2202–2211.
[22] R. Banerjee, S.G. Kandlikar, ECS Trans. 41 (2011) 489–497.
[23] M.V. Williams, E. Begg, L. Bonville, H.R. Kunz, J.M. Fenton, J. Electrochem. Soc. 151 (2004) A1173–A1180.
[24] N. Zamel, N.G.C. Astrath, X. Li, J. Shen, J. Zhou, F.B.G. Astrath, H. Wang, Z. Liu, Chem. Eng. Sci. 65 (2010) 931–937.
[25] Z. Fishman, J. Hinebaugh, A. Bazylak, J. Electrochem. Soc. 157 (2010) B1643–B1650.
[26] I.M. Hutten, Handbook of Nonwoven Filter Media, Elsevier Ltd., Oxford, UK, 2007.
[27] M.M. Tomadakis, T.J. Robertson, J. Compos. Mater. 39 (2005) 163–188.
[28] C.N. Davies, Proc. Inst. Mech. Eng. B1 (1952) 185–198.
[29] M.M. Tomadakis, S.V. Sotirchos, AIChE J. 39 (1993) 397–412.